ORIGINAL ARTICLE

Chemistry-led investigations into the mode of action of NAMPT activators, resulting in the discovery of non-pyridyl class NAMPT activators

Siyuan Tang[a], Miguel Garzon Sanz[a], Oliver Smith[a],
Andreas Krämer[b,c,d,e], Daniel Egbase[f], Paul W. Caton[f],
Stefan Knapp[b,c,d,e], Sam Butterworth[a,*]

[a]*Division of Pharmacy and Optometry, School of Health Sciences, Manchester Academic Health Sciences Centre, University of Manchester, Manchester M13 9PL, UK*
[b]*Structural Genomics Consortium (SGC), 60438 Frankfurt Am Main, Germany*
[c]*Buchmann Institute for Life Sciences (BMLS), 60438 Frankfurt Am Main, Germany*
[d]*Institut für Pharmazeutische Chemie, Goethe University, 60438 Frankfurt Am Main, Germany*
[e]*Frankfurt Cancer Institute (FCI), 60596 Frankfurt Am Main, Germany*
[f]*Department of Diabetes, School of Cardiovascular and Metabolic Medicine & Sciences, Faculty of Life Sciences & Medicine, King's College London, London SE1 1UL, UK*

Abstract The cofactor nicotinamide adenine dinucleotide (NAD^+) plays a key role in a wide range of physiological processes and maintaining or enhancing NAD^+ levels is an established approach to enhancing healthy aging. Recently, several classes of nicotinamide phosphoribosyl transferase (NAMPT) activators have been shown to increase NAD^+ levels *in vitro* and *in vivo* and to demonstrate beneficial effects in animal models. The best validated of these compounds are structurally related to known urea-type NAMPT inhibitors, however the basis for the switch from inhibitory activity to activation is not well understood. Here we report an evaluation of the structure activity relationships of NAMPT activators by designing, synthesising and testing compounds from other NAMPT ligand chemotypes and mimetics of putative phosphoribosylated adducts of known activators. The results of these studies led us to hypothesise that these activators act *via* a through-water interaction in the NAMPT active site, resulting in the design of the first known urea-class NAMPT activator that does not utilise a pyridine-like

warhead, which shows similar or greater activity as a NAMPT activator in biochemical and cellular assays relative to known analogues.

1. Introduction

Nicotinamide adenine dinucleotide (NAD^+) and its reduced and/or phosphorylated forms are essential cofactors for a range of both redox and non-redox based processes in healthy cells[1]. Declining NAD^+ levels are associated with aging and have been implicated in age-associated disease including neurodegeneration and metabolic disease, with *in vivo* studies demonstrating the potential role of increasing NAD^+ in improving healthy aging in animal models[2,3].

As a result, the enhancement of NAD^+ levels by either nutritional or pharmacological approaches is a potential therapeutic option for treatment of aging-associated conditions[2]. While cells have multiple routes by which NAD^+ can be obtained, the salvage pathway, in which nicotinamide and phosphoribosyl pyrophosphate are condensed to form the NAD^+ precursor nicotinamide mononucleotide (NMN) by the action of nicotinamide phosphoribosyl transferase (NAMPT), is the most studied pathway in the context of cellular control of NAD^+ levels[4,5].

NAMPT is a highly conserved homo-dimeric protein containing two identical active sites that each comprise residues from both chains of the dimer[4]. It catalyses the reaction between phosphoribosyl pyrophosphate (PRPP) and nicotinamide (NA) to form NMN and pyrophosphate (PP), with NMN then further converted to NAD^+ by the action of Nicotinamide mononucleotide adenosyl transferase (NMNAT), which catalyses the

condensation of NMN and adenosine triphosphate (ATP, Fig. 1)[4]. The catalytic activity of NAMPT is dependent on ATP, which binds in the catalytic site resulting in phosphorylation of His247[4]. This phospho-histidine is readily hydrolysed under physiological conditions and can also facilitate the transfer of phosphate to ATP to form ATtP[6]. Due to the high activity of NMNAT and high levels of NMNAT and ATP in cells, NAMPT-mediated NMN synthesis is considered the rate-limiting stage of the NAD^+ salvage pathway[7].

The understanding of cellular function of this pathway was driven in part by the discovery of highly cytotoxic NAMPT inhibitors, the prototypical example of which is FK866 **1** (Fig. 2)[9]. Subsequent research has identified a number of NAMPT inhibitor chemotypes, which can be classified into two broad sets; pyridine-like inhibitors, such as FK866 and compound **2** (Fig. 2), which react with PRPP in the active site to form high affinity phosphoribosylated adducts (exemplified by **3**, Fig. 2), and reversible non-substrate inhibitors such as compound **4** (Fig. 2)[10−12]. These inhibitors are able to induce near complete depletion of NAD^+ in cells within 24 h of treatment, leading to metabolic dysfunction including loss of ATP after 12−24 h, and typically induce cell death after 72−96 h[9]. As a result, NAMPT inhibitors have been extensively studied, especially in the oncology setting, however due to the relative non-specificity of these molecules across different cell types such compounds have only been advanced to clinical trials in oncology indications and to date none have shown a useable therapeutic window[13].
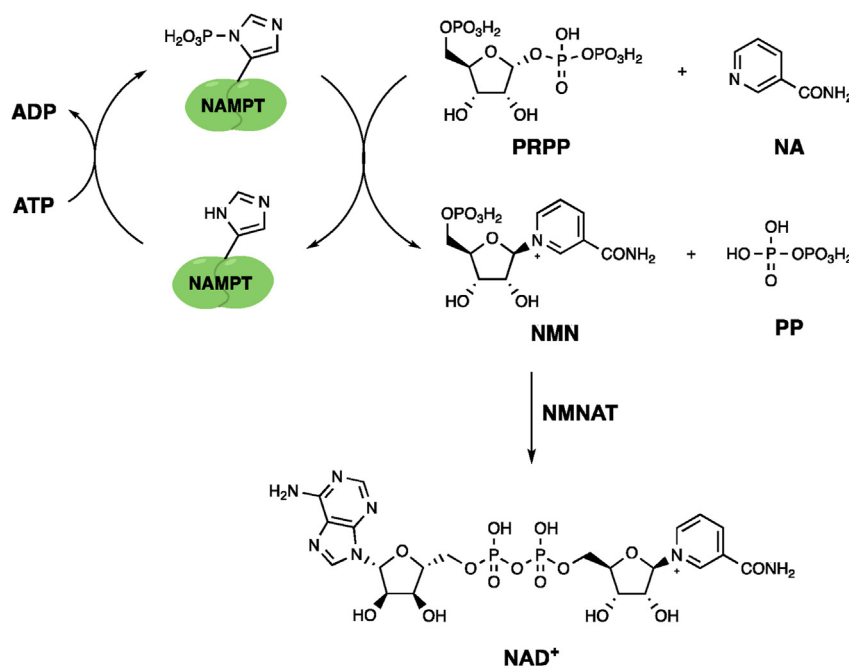
Figure 1   The role of NAMPT in the NAD^+ salvage pathway[4,8].
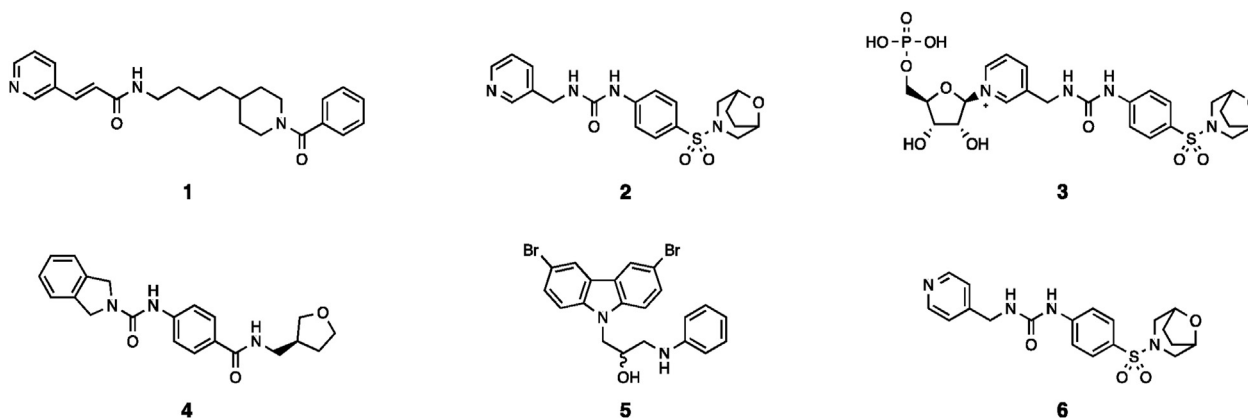
Figure 2 Structures of previously reported NAMPT modulators. Compounds **1**, **2**, **3** and **4** are NAMPT inhibitors, compounds **5** and **6** are reported to be NAMPT activators, despite **6** being a close analogue of inhibitor **2**.

As NAMPT function is the rate limiting step in the NAD$^+$ salvage pathway, it is possible that compounds that can enhance cellular NAMPT activity could be used to increase cellular NAD$^+$ levels and thus treat conditions associated with reduced NAD$^+$ function. The first identified example of such a molecule is P7C3 **5** (Fig. 2), which can increase cellular NAD$^+$ levels and may be a direct NAMPT ligand, however we and others have failed to detect a direct interaction between P7C3 and NAMPT by biophysical methods[14−16]. A more recent study identified SBI-797812 **6** (Fig. 2) as a direct NAMPT ligand that is capable of activating the enzyme *in vitro* and results in increased NAD$^+$ levels in cells and mouse *in vivo* studies[15]. The mechanism of these compounds appears to be linked to altered reactivity of phospho-His247[15], however it is not clear if this is the result of binding to one active site resulting in activation of the second free site, or through competitive reversible binding at the functional active site which results in net activation of the protein.

The structure and published structure−activity relationships around **6** are somewhat surprising given the compounds similarity to potent NAMPT inhibitors such as **2** (Fig. 2). There appears to be a specific requirement for a pyridine-like nitrogen at the 4-position of **6**, with the phenyl analogue being inactive and the 3-pyridyl being a known NAMPT inhibitor. This pyridine-like nitrogen is also present in all urea-class NAMPT activators reported in later publications, wherein the 3-pyridine has been modified to heterocyclic systems including pyrazoles and isoxazoles, alongside modifications in other regions that can enhance both activity and selectivity

of these compounds[17−19]. This finding has been followed by the discovery of further NAMPT-activator chemotypes that do not bind in the NA site, however the pyridine/azole urea molecules remain the most fully biologically characterised molecules[20].

2. Results and discussion

As a result of the limitations in our understanding of the activity of **6** and related NA-site binding activators, we sought to investigate the structure−activity relationships around this compound in more detail by preparing analogues based on the following design criteria:

1) To date, the published examples of NAMPT-activators from the NA-site binding class are based on the urea-like scaffold of **6**[17−19]. Crystal structures of closely related inhibitors such as **2** demonstrate a similar binding mode to FK866 and triazole-based NAMPT inhibitors, we therefore designed and synthesised compounds **7** and **8** (Fig. 3) to investigate the activity of compounds from other scaffolds.
2) Given the essential nature of the 4-pyridyl like functionality in **6** and analogues, we hypothesised these compounds may form phosphoribosylated adducts, in a similar manner to the conversion of inhibitor **2** to adduct **3**. While the detection of such a species has not been disclosed and we observed no evidence of its formation by LC−MS *in vitro*, we considered it possible that very low levels of a high affinity phosphoribosylated species could be responsible for the observed activity, as it is known
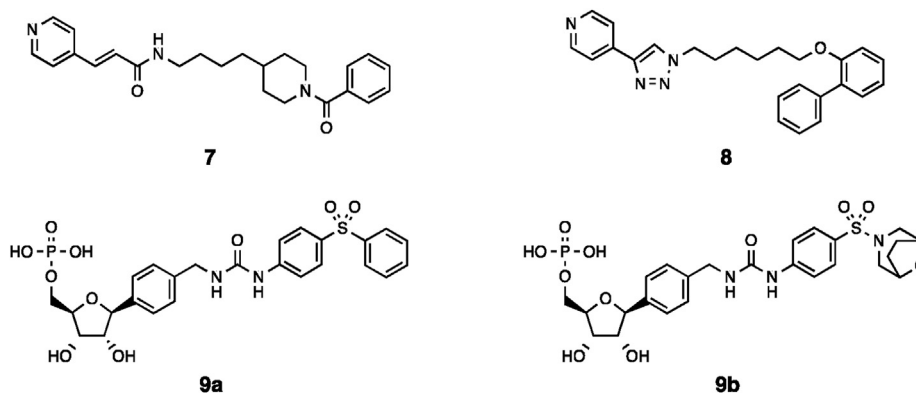
Figure 3 Structures of tool compounds designed to investigate mechanism of NAMPT activators.
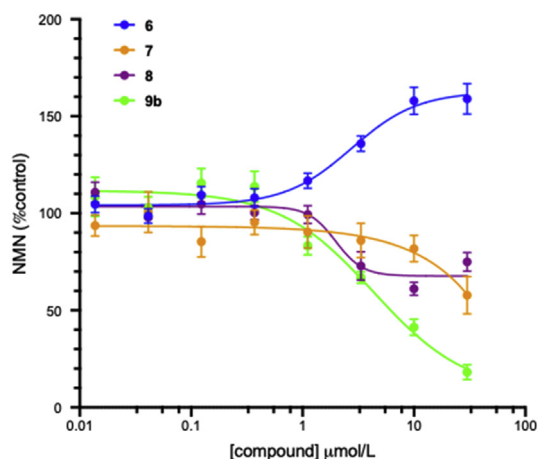
Figure 4 Effects of compounds **6**, **7**, **8** and **9b** on NMN production in the biochemical NAMPT assay. All data is from a minimum of three independent replicates conducted in triplicate and is shown as mean ± SEM.

that the conformation of such phosphoribosylated analogues affects their affinity and rate of formation[10]. To avoid any concerns around stability of the phosphoribosylated analogue, we designed and synthesised the stable C-nucleoside derivatives **9a** and **9b** (Fig. 3) as stable analogues of the product derived from phosphoribosylation of **6**.

The activity of known activator **6** and new analogues **7**, **8** and **9b** (Fig. 3) were initially assessed in a biochemical assay similar to that reported previously[21]. This assay format allows for detection of both activators and inhibitors of NAMPT, however

in our hands the assay-to-assay variability is higher for activators than inhibitors. In our experiments, **6** increases NAMPT activity, resulting in a 59% increase in NMN production at 30 µmol/L, with an EC_{50} of 2.75 µmol/L, which represents lower activity than the reported EC_{50} of 0.37 µmol/L with maximal 110% activation.

Compounds **7** and **8**, based on alternative NAMPT inhibitor scaffolds, both act as weak inhibitors in this assay, suggesting that the urea-derived **6** and analogues have a unique mechanism or binding mode which are distinct from these structural classes. The weak activity of these compounds relative to the reported low-nmol/L IC_{50} of the related 3-pyridiyl analogues is consistent with them either not acting as substrates or forming low affinity phosphoribosyl adducts. Consistent with this observation, the phosphoribosylated analogue **9b** also showed no evidence of activation, but rather acts as a weak inhibitor of NAMPT, with an IC_{50} of 4.32 µmol/L (Fig. 4).

While this data alone is not conclusive, the inhibitory effect of the phosphoribosyl mimetic **9b** suggests that NAMPT activation by **6** and analogues is not mediated by phosphoribosylated adducts generated by the action of NAMPT.

As part of our studies on NAMPT activators compound **9a**, a close analogue of **9b** which differs only in a solvent-adjacent region away from the active site, had previously been co-crystallised with NAMPT and as expected interacts in the active site, however there are some key differences relative to the majority of previously reported NAMPT-ligand structures. Firstly, the phosphoribose is displaced from the region occupied by the natural substrate/products or known phosphoribosylated inhibitor structures, which is likely due to the change in orientation enforced by the switch from 3- to 4-substitution (Fig. 5). The second observed change is a shift of the orientation of the nicotinamide-like phenyl ring such that it no longer
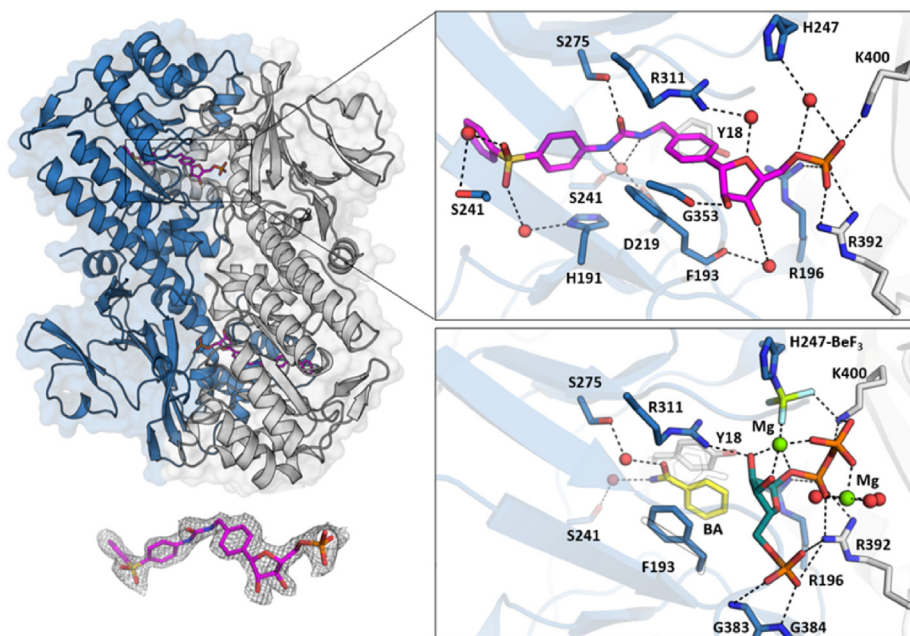
Figure 5 Compound **9a** bound to dimeric NAMPT (PDB: 7Q8T). One chain is colored in blue the other in grey. The upper insert shows detailed interaction of **9a** (pink) with surrounding residues as dashed black lines. Bridging water molecules are shown as red spheres. The bottom right insert shows the PRPP (teal) and nicotinamide mimetic (benzamide, BA, yellow) bound structure of BeF$_3$-His247 (PDB: 3DKL). Magnesium ions are coloured in green. The orientation is the same as in the upper panel. The conformation change of F193 and Y18 is indicated as a black outline. Bottom right shows the observed electron density of the ligand contoured at 1 σ.
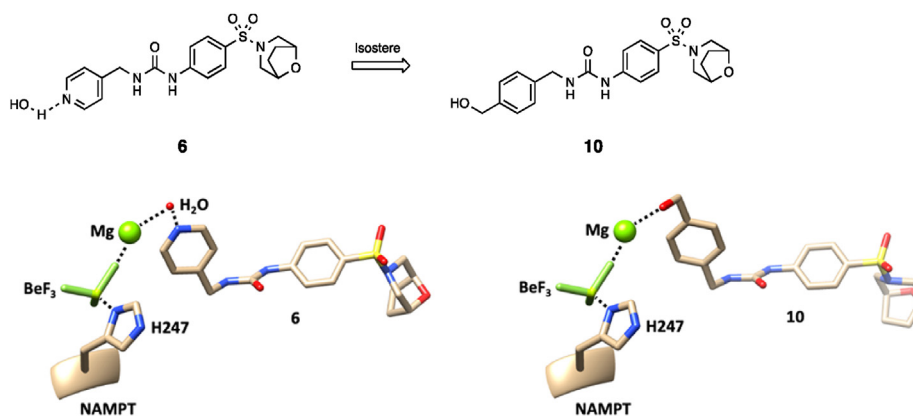
Figure 6 Design hypothesis of benzyl alcohol **10** as an isostere of a putative pyridine−water interaction made by **6**. Docked pose of compounds **6** and **10** bound to PDB:7Q8T, aligned with the His 247-BeF$_3$-Mg residues from PDB: 3DKL, demonstrating the potential for interactions with the p-His247 region in this binding mode. All other NAMPT residues from PDB:7Q8T and PDB: 3DKL are removed for clarity.

makes pi-interactions with Phe193 and Tyr18 (as are observed with NMN and the majority of NAMPT-inhibitor structures), but rather sits in a pocket between Phe193 and Arg 311, forming an apparent pi-stacking interaction between the phenyl ring in **9a** and the cationic guanidine of Arg311 (Fig. 5). This binding mode is closer to that previously observed in the complex with an ADP analogue, while both Phe193/Tyr18 and Phe193/Arg311 binding modes are observed in the structure of the phosphoribosylated urea-based inhibitor SAR154782 (PDB: 5LX5)[22,23].

Effectively all known NAMPT inhibitors form either direct or water-mediated hydrogen bonding interactions in the region of Asp219, Ser241 and Arg311, for example these interactions are achieved by the urea of **2** and the secondary amide of FK866. These interactions are maintained by **9a** with the change in binding mode to Phe193/Arg311 resulting from flexibility in the aryl−CH$_2$−urea region, which is a unique feature of this ligand class relative to other NAMPT inhibitor chemotypes.

As compounds **7** and **8** show inhibitory activity against NAMPT, both the Phe193/Arg311 binding mode and NAMPT activation appear to be a unique feature of the CH$_2$-urea class ligands. We therefore hypothesised that the known NAMPT activators may bind specifically through this binding mode, however this binding mode alone cannot explain the switch in activity as both **9b** and SAR154782 are inhibitors of the protein.

To further understand the potential link between the Phe193/Arg311 binding mode and NAMPT activation, we examined the structure of **9a** overlaid with the structures of NAMPT bound to its substrates, including the phospho-histidine mimetic BeF$_3$-His247 structure. This analysis revealed that the ribose ring oxygen in **9a** occupies a position in the active site which is very close to the ribose hydroxyls in the product-bound BeF$_3$-His247 structure.

Given the lack of obvious rationale for the requirement for the 4-pyridyl (or 3-azole) ring in **6** and analogues, we docked **6** into NAMPT in the conformation seen with **9a**. This docking resulted in a close overlay with the benzyl urea region of **9a**, with the pyridine of **6** orientated towards His247 but not in a region that would allow for any direct interactions with the protein (Fig. 6). We considered the possibility that this nitrogen forms an indirect (*i.e.*, through-water) interaction with p-His247 or a metal ion (likely magnesium) thereby stabilising the phospho-histidine and/ or holding the enzyme in a conformation that favours the formation of NMN at the second active site. Overlay with the His247-BeF$_3$-Mg bound NAMPT structure from PDB:3DKL demonstrated this interaction is feasible (Fig. 6).

Based on the findings that: 1) Both NAMPT activation and the Phe193/Arg311 binding mode are unique features of the benzyl urea NAMPT ligand chemotype, 2) the 4-pyridyl (or 3-azole) functionality that is essential for NAMPT activation in this
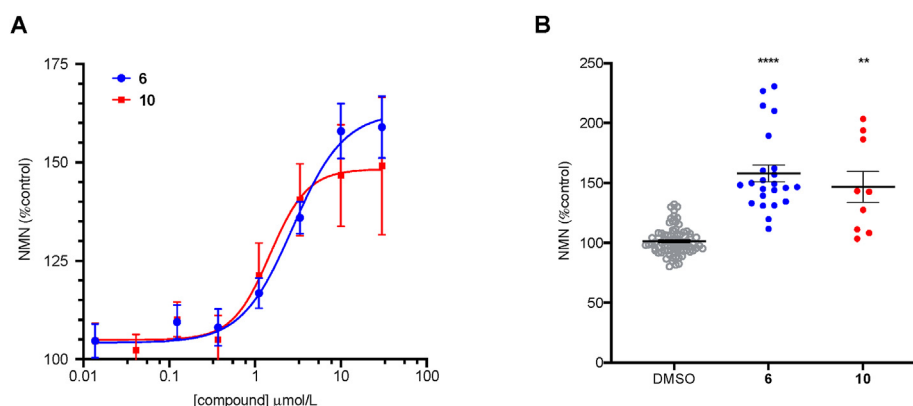
Figure 7 Effects of compounds **6** and **10** on NMN production in the biochemical NAMPT assay; (A) Dose response data. All data is from a minimum of three independent replicates conducted in triplicate and is shown as mean ± SEM (B) Comparison of effects of **6** ($n = 21$) and **10** ($n = 9$) at 10 μmol/L *vs* DMSO control ($n = 81$). Significant differences (from DMSO vehicle) are denoted by **$P < 0.01$ and ****$P < 0.0001$.
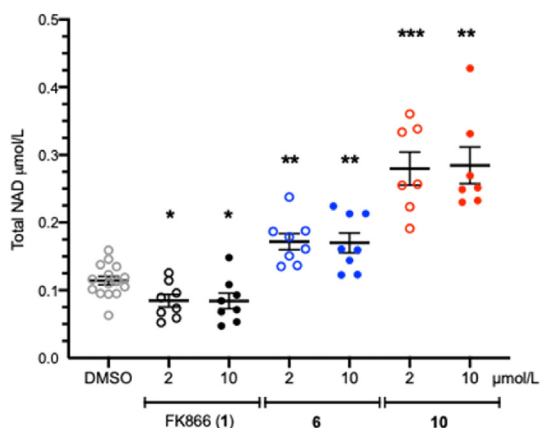
Figure 8 Effects of 4-h treatment of FK866 (**1**) and compounds **6** (blue) and **10** (red) on NAD^+ levels in A549 cells. Significant differences (from DMSO vehicle) are denoted by $*P < 0.05$, $**P < 0.01$ and $***P < 0.001$.

chemotype does not appear to be linked to formation of phosphoribosylated adducts and 3) the Phe193/Arg311 binding mode places the essential 4-pyridyl (or 3-azole) in a region that would allow formation of water-mediated interactions with the p-His247, we designed compound **10**, with the aim that the benzylic alcohol can directly replicate this putative interaction (Fig. 6). The use of benzyl alcohols as bioisosteres for a pyridine−water interaction (or the reverse) is precedented, for example in the design of PI3K inhibitors, and has the advantage of reducing the likelihood of CYP450 interactions which are commonly observed with unsubstituted aza-hetrocycles[24].

Compound **10** was therefore prepared and tested in the NAMPT activity assay used previously. The results from these experiments demonstrate that benzylic alcohol **10** retains the ability to enhance NMN production by NAMPT, with an observed EC_{50} of 1.49 μmol/L under these conditions (Fig. 7). This result is consistent with the hypothesis that **6** and related molecules make an interaction with a water molecule in the active site of NAMPT

(potentially interacting with coordinated metal in the active site) and, as this compound cannot be a substrate, further supports the hypothesis that the activity of **6** is not dependant on phosphoribosylation.

Following the characterization of **10** as a novel NAMPT activator in biochemical experiments, we sought to evaluate its effects on NAD^+ levels in cells following similar methods to those utilized in the characterization of **6**[15]. A 4-h treatment of A549 cells with compounds **6** or **10** results in a significant increase in total NAD^+/NADH levels relative to media control (DMSO). At the tested concentrations of 2 and 10 μmol/L compound **10** demonstrated a higher degree of activity relative to the known activator **6**, increasing NAD^+/NADH levels by an average of 247% *vs* 150% (difference reaches significance at $P < 0.01$ at both concentrations, Fig. 8).

Following the report that NAMPT activators enhance insulin secretion *in vivo* and based on our previous interest in the role of NAMPT in this context, we sought to investigate the effects of compounds **6** and **10** on *ex vivo* mouse islets[19,25]. In line with our results in A549 cells compound **10** caused a dose dependant increase in total NAD^+ content, reaching 310% control at 5 μmol/L (Fig. 9A), which resulted in increased insulin secretion response at higher concentrations following stimulation with 20 mmol/L glucose (Fig. 9B). Also similar to the data in A549 cells, compound **6** showed more limited effects on islets, with increase in NAD^+ levels to 142% of control and no significant effect on insulin secretion (data not shown).

Chemistry. Compounds **6**, **8** and **10** were synthesised from known intermediates **11** and **12** respectively by following published protocols (Scheme 1)[15,26]. Likewise, previously reported intermediate **13** was utilised to synthesise **14**, which was coupled to the pyridine warhead through a Heck reaction to generate compound **7** (Scheme 1)[27].

To synthesise **9a**, we started by converting commercially available aniline **15** to carbamate **16** by following a similar protocol to that used previously[15]. Ribonolactone **17** was alkylated to form **18** as a mixture of isomers and deoxygenation gave nucleoside **19** as a single diastereoisomer, in accordance with the
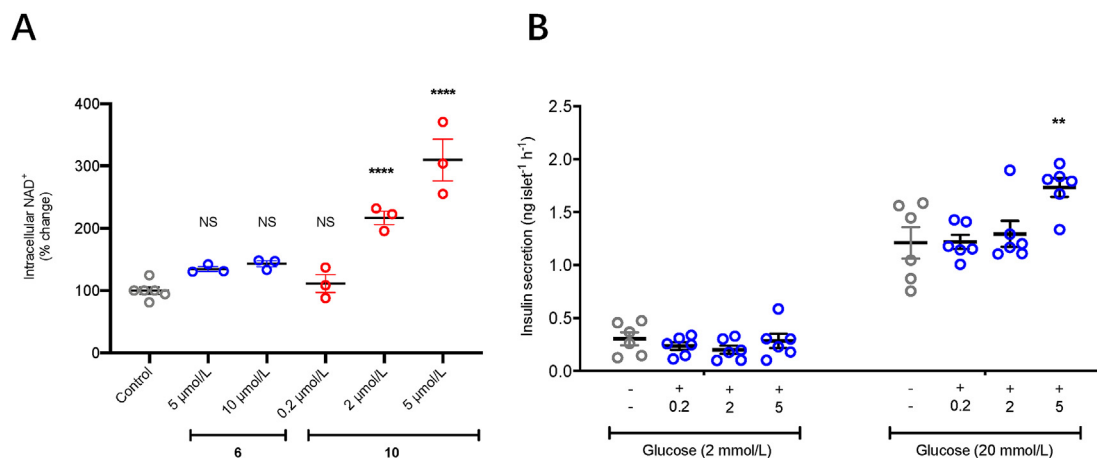
Figure 9 (A) Effects of compounds **6** and **10** on intracellular NAD^+ change in mouse CD1 islets. Data is from three independent replicates. (B) Effects of compounds **6** on insulin secretion from mouse CD1 islets. Data is from three independent replicates conducted in duplicate. All data is shown as individual values with mean ± SEM ($n = 6$). Significant differences (from control) are denoted $**P < 0.01$ and $****P < 0.0001$ by one-way ANOVA followed by Dunnett's multiple comparisons test.
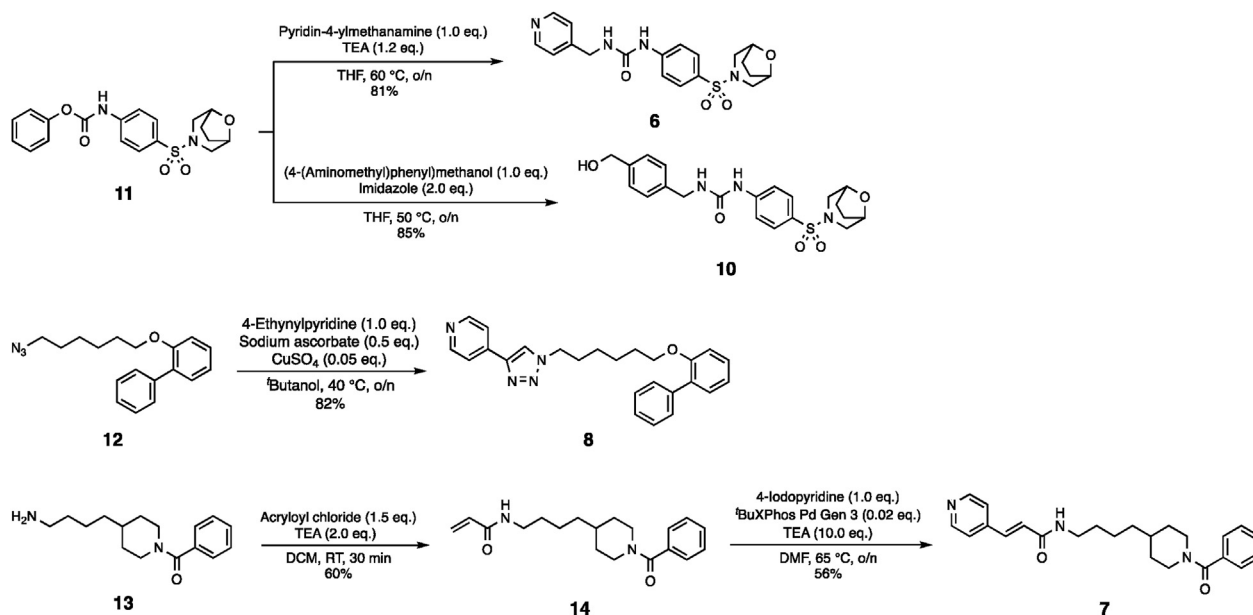
Scheme 1   Synthetic protocol of compounds **6**, **7**, **8** and **10**.

established selectivity of this rection[28]. **19** was debenzylated to compound **20** using published conditions[28], then converted to acetal **21**. Subsequent phosphorylation reaction generated **22**, which was reduced to the corresponding amine **23** using borane[29–33]. The sugar warhead **23** was reacted with the previously synthesised carbamates **16** and **11** to afford the protected intermediates **24a** and **24b**, which were deprotected to provide the desired compounds **9a** and **9b** respectively (Scheme 2) [34,35].
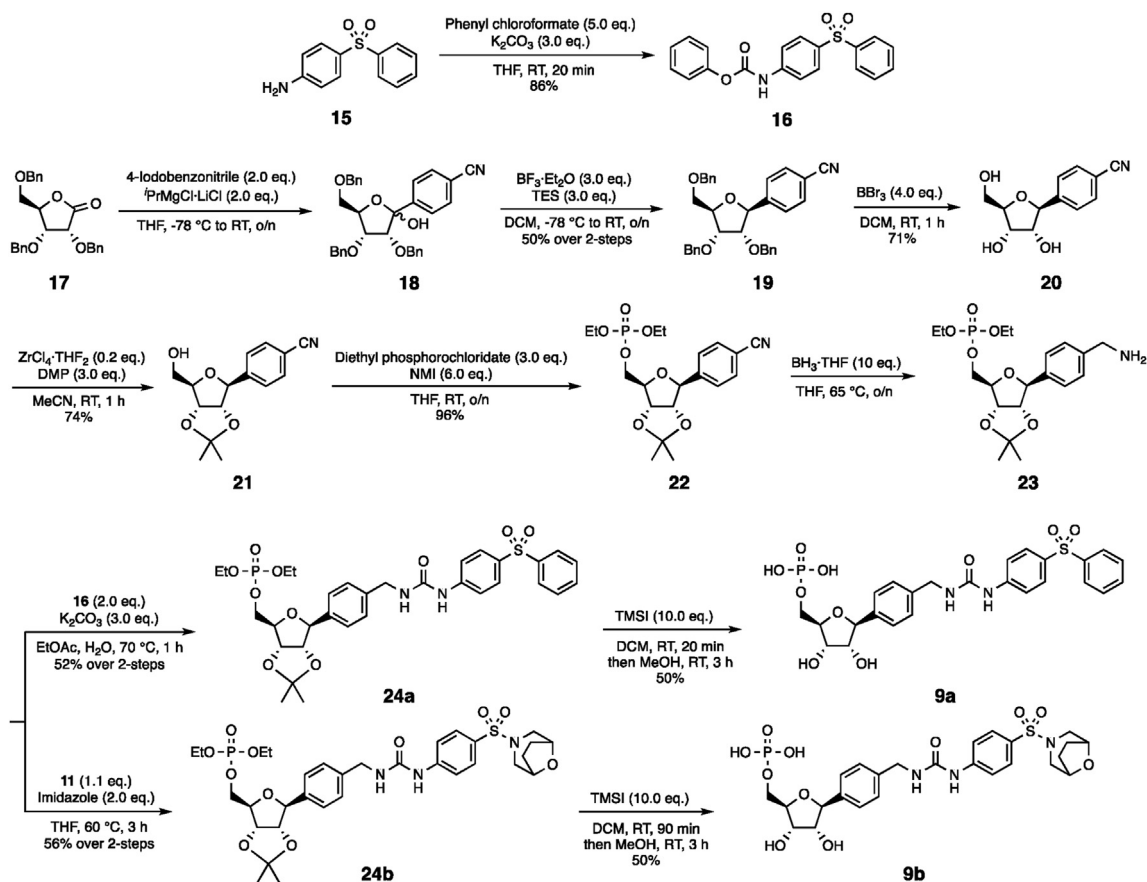
Scheme 2   Synthetic protocol for compounds **9a** and **9b**.

Table 1 Gradient used on a standard 4-min run with a 0.60 mL/min flow rate for LC−MS.

Time (min)	MeCN in water (% v/v)
0 to 0.50	5:95
0.50 to 2.50	5:95 to 95:5
2.50 to 3.00	95:5
3.00 to 3.10	95:5 to 5:95
3.10 to 4.00	5:95

3. Conclusions

Enhancing NAD$^+$ levels represent a potential therapeutic strategy for treatment of a range of diseases associated with aging. The analysis of the structure−activity relationships (SAR) and binding mode of molecules that combine the structural features of known NAMPT activators and inhibitors conducted here reveals areas clearly divergent SAR, highlighting likely changes in the binding mode between chemically related NAMPT activators and inhibitors. The hypothesis that the critical 4-pyridiyl (or azahetrocycle) in such compounds makes a water mediated interaction with NAMPT, or more probably an interaction bridged by a NAMPT-chelated magnesium ion, led to the design of a novel NAMPT activator warhead which demonstrates equivalent or superior activity to the pyridines in *in vitro* models. This work will inform further studies and optimisation to provide drug-like and ultimately clinically developable NAMPT activators.

4. Experimental

4.1. Expression and purification of NAMPT

The plasmid containing the NAMPT (from *Mus musculus)* along with an N-terminal His$_6$-Tag and TEV cutting site was transformed into *E. coli* Rosetta cells. The cells were grown in Terrific Broth medium containing ampicillin. Protein expression was induced at an OD$_{600}$ of ∼2 by using 0.5 mmol/L, isopropyl-thio-galactopyranoside (IPTG) at 18 °C. The next morning cells were harvested by centrifugation (6000×g). Typically, 20 g of cells were resuspended in lysis buffer (50 mmol/L HEPES pH 7.5, 500 mmol/L NaCl, 5% glycerol, 1 mmol/L TCEP, 20 mmol/L imidazole) and subsequently disintegrated by sonication on ice. Cell fragments were separated by centrifugation (30 min, 21,000×g, 4 °C) and the supernatant was loaded onto an immobilized metal affinity sepharose resin (Chelating Sepharose™ Fast Flow, GE Healtcare, Uppsala, Sweden) pre-equilibrated with 30 mL lysis buffer. After washing the resin with ∼100 mL lysis buffer, the protein was eluted by an imidazole step gradient (50, 100, 200, 300 mmol/L). Fractions containing protein were pooled together and dialysed overnight against 1 L of final buffer (25 mmol/L HEPES pH 7.5, 200 mmol/L NaCl, 5% glycerol, 0.5 mmol/L TCEP) at 4 °C. Additionally, TEV protease was added (protein:TEV ∼20:1 molar ratio) to cleave the tag. The protein solution was loaded onto Nickel-Sepharose beads again to remove TEV protease and uncleaved protein. The flow through fraction was concentrated to approx. 4−5 mL and loaded onto Superdex 200 16/60 HiLoad size-exclusion chromatography (SEC) column equilibrated with final buffer. Following elution of the protein the pure fractions were combined and concentrated to approximately 20 mg/mL.

4.2. Crystallisation

NAMPT was co-crystallized using the sitting-drop vapour diffusion method by mixing protein (4−6 mg/mL), inhibitor of interest (0.5−1 mmol/L) and reservoir conditions in 2:1, 1:1, and 1:2 ratios at 20 °C. Crystals appear after 1 day in reservoir solution containing 20%−30% PEG 3350, 0.1 mol/L NaCl, 0.1 mol/L HEPES, pH 8.2.

4.3. Enzyme activity assay

The enzymatic assay was adapted from a published protocol[21]. NAMPT (36 nmol/L) with PRPP (50 μmol/L) and ATP (2 mmol/L) in TMD buffer (50 mmol/L Tris-HCl, 10 mmol/L MgCl$_2$, 2 mmol/L DTT, pH 7.5) were incubated at 37 °C for 20 min in 96-well opaque bottom plate (final volume 180 μL per well). The reactions were performed in the presence of NAMPT activators, inhibitors or DMSO control with the final DMSO concentration was 1% in all cases. After 20 min incubation at 37 °C, NAM (10 μL of 125 μmol/L solution in TMD buffer, to give a final concentration of 25 μmol/L) was added to each well and further incubated for 20 min at 37 °C[15]. NMN was assayed using a chemical method which converts NMN into a fluorescent derivative by mixing NMN-containing samples with 20 μL of 20% acetophenone (in DMSO) and 20 μL of 2 mol/L KOH aqueous solution. Following regent addition, the mixture was kept for 5 min at ambient temperature then 90 μL of 80% formic acid was added to each sample. Fluorescence was measured using a Hidex sense microplate reader with excitation filter 355 ± 40 nm and emission 460 ± 20 nm, and NMN concentrations calculated using a NMN calibration curve performed in the same plate.

4.4. Cellular studies

Human A549 lung carcinoma cells were grown in RPMI 1640 medium (with 1% L-glutamine), 10% fetal bovine serum (T175 cell culture flasks). Plated in 96-well plates (white plate, clear bottom with lid, Costar, Cat.# 3610) at approximately 800 cells per well in 50 μL of medium and treated with testing compounds or DMSO (control) for 4 h at 37 °C. After the incubation, plates were equilibrated to ambient temperature and 50 μL of NAD/NADH-Glo™ Assay solution (Promega, Cat.#G9071) was added. Plates were incubated at ambient temperature for 1 h and luminescence was measured using a plate reader (FLUOstar OPTIMA, BMG Labtech). NAD$^+$/NADH concentrations were calculated using an NAD$^+$ calibration curve performed in the same plate.

4.5. Molecular docking

To reveal the binding model of compounds **6** and **10**, we built a complex of compounds **6**, **10** and NAMPT based on the crystal structures of NAMPT with compound **9a** (PDB code: 7Q8T) and published PRPP-bound structure of BF$_3$-His247 NAMPT (PDB code: 3DKL). Compound **9a** was removed from the crystal structure and all hydrogen atoms added. The chemical structures of compounds **6** and **10** were sketched in SYBYL (Tripos, St Louis, MO, USA) and protonated, if appropriate, before energy minimization using the Tripos force field (Gasteiger−Hückel charges, distance-dependent dielectric constant = 4.0, nonbonded interaction cutoff = 8 Å and termination criterion = energy gradient <0.05 kcal/(mol × Å) for 10,000 iterations). The

molecular docking was performed using GOLD Suite 5.1 (Cambridge Crystallographic Data Centre, Cambridge, UK). The original ligand was extracted and the new ligands (compounds **6** and **10**) were fit into the binding pocket of compound **9a** in NAMPT. The ChemScore and GoldScore fitness scoring functions were utilized to identify lowest energy binding poses. The exported complexes were edited using UCSF Chimera 1.13.1 software.

4.6. General chemistry experimental

Commercial reagents and solvents were used directly without further purification. Anhydrous solvents were supplied by Acros Organics over 4 Å molecular sieves. Glassware such as round bottom flasks and ace pressure tubes were dried in the oven first and then heated with a heating gun under vacuum. Progress of the reaction was monitored with TLC using F_{245} aluminium-backed silica gel plate purchased from Merck. UV light (254/365 nm) and $KMnO_4$ were used for visualisation. The following cooling baths were used: 0 °C (ice/water), −10 °C (ice/MeOH), −40 °C (dry ice/MeCN) and −78 °C (dry ice/acetone). For heating reactions, paraffin oil baths and stirrer hotplates were employed and the temperature was monitored using a thermometer. Compounds were purified by flash column chromatography (silica gel) using Geduran silica gel 60 or reverse phase flash column chromatography CombiFlash® machine using 5.5, 15.5 or 30.0 g C18 Gold columns with 20−40 μm silica, eluting with a gradient 0%−100% MeCN in water as acid method (0.1% formic acid as modifier) or base method (0.1% NH_4OH as modifier) as indicated, or by prep HPLC using C18 Kinetex HPLC column with 5 μm silica, eluting with a gradient 0%−100% MeCN in water. Infrared (IR) spectra were recorded on a Bruker Tensor 27 FT-IR using an ATR attachment. NMR spectra were recorded on a Bruker AV400 (^{1}H = 400 MHz, ^{13}C = 101 MHz, ^{19}F = 376 MHz, ^{31}P = 162 MHz) spectrometer in commercial deuterated solvents. Chemical shift (δ) were reported in ppm and spectra were recorded in $CDCl_3$ referenced to residual $CHCl_3$ (δ_H 7.26 ppm, δ_C 77.16 ppm), CD_3OD referenced to residual MeOH (δ_H 3.31 ppm, δ_C 49.00 ppm) or $(CD_3)_2SO$ referenced to residual DMSO (δ_H 2.50 ppm, δ_C 39.52 ppm). Coupling constants J were reported in Hz to the nearest 0.1 Hz. Coupling constants that were non-identical were reported as averages. Data were processed on Mestrenova 14.0.1. Unless stated otherwise, ^{31}P were reported decoupled to ^{1}H, ^{19}F were reported coupled to ^{1}H. All ^{1}H and ^{13}C assignments were supported by two-dimensional spectrum ^{1}H−^{1}H COSY, ^{1}H−^{1}H NOESY, ^{1}H−^{13}C HSQC and ^{1}H−^{13}C HMBC. LC data was obtained using a Waters ACQUITY UPLC PDA detector scanning between 210 and 400 nm. LC−MS retention time was reported at t_R in minutes. Mass spectra were recorded on Waters ACQUITY QDa detector. All solvents were LC−MS grade (Fisher Optima) and were modified by the addition of 0.1% formic acid (Fisher Optima) as acid method or NH_4OH (Fisher, 28% v/v aq. solution) as base method as indicated. Table 1 detailed the gradient used on a standard 4-min run with a 0.60 mL/min flow rate. All high-resolution mass spectrometry (HRMS) was performed on a Thermofisher Exactive Plus EMR Orbitrap.

1-(4-((8-Oxa-3-azabicyclo[3.2.1]octan-3-yl)sulfonyl)phenyl)-3-(pyridin-4-yl)urea (6).

11 (80 mg, 0.21 mmol) was dissolved in THF (10 mL), pyridin-4-ylmethanamine (22 mg, 0.21 mmol) and TEA (3.45 × 10^{-2} mL, 0.25 mmol) were added under argon atmosphere. The mixture was heated up to 60 °C and stirred overnight under argon atmosphere. The reaction mixture was extracted with EtOAc (3 × 30 mL) and the organic phases were combined, dried over $MgSO_4$, filtered and concentrated under reduced pressure to provide a yellow oil. The crude material was purified by flash chromatography (silica gel), eluting with 3% MeOH in DCM to afford the title compound (69 mg, 0.17 mmol, 81%) as a colorless oil. ^{1}HNMR (400 MHz, $CDCl_3$) δ_H 9.35 (s, 1H), 8.53−8.47 (m, 2H), 7.693−7.62 (m, 2H), 7.56 (d, 2H, J = 8.7 Hz), 7.323−7.26 (m, 2H), 6.98 (t, 1H, J = 6.1 Hz), 4.33 (dd, 4H, J = 12.9, 4.1 Hz), 3.20 (d, 2H, J = 11.0 Hz), 2.38 (dd, 2H, J = 11.3, 2.3 Hz), 1.78 (d, 4H, J = 2.5 Hz). ^{13}CNMR (101 MHz, $CDCl_3$) δ_C 154.9, 149.6, 149.3, 145.0, 128.8, 126.2, 122.0, 117.3, 72.8, 50.9, 41.9, 27.5. MS *m/z* (ES$^+$) 403.4 [M+H]$^+$.

(E)-N-(4-(1-Benzoylpiperidin-4-yl)butyl)-3-(pyridin-4-yl) acrylamide (7).

4-Iodopyridine (33 mg, 0.16 mmol) was dissolved in anhydrous DMF (3 mL), **14** (50 mg, 0.16 mmol), ^{t}BuXPhos Pd Gen-3 (25 mg, 0.03 mmol) and TEA (0.22 mL, 1.60 mmol) were added under argon atmosphere. The mixture was stirred at 65 °C overnight under argon atmosphere. The reaction mixture was quenched with water (30 mL) and extracted with EtOAc (3 × 20 mL) and the organic phases were combined, dried over $MgSO_4$, filtered and concentrated under reduced pressure to provide a brown oil. The crude material was purified by CombiFlash® using acid method to afford the title compound (35 mg, 0.09 mmol, 56%) as a colourless oil. V_{max} (thin film, ATR)/cm^{-1}: 3057, 2180, 1968, 1671, 1625, 1552, 1445, 1341, 1282, 1224, 1113, 979, 814, 708, 543. ^{1}HNMR (400 MHz, $CDCl_3$) δ_H 8.52−8.46 (m, 2H), 7.42 (d, 1H, J = 15.6 Hz), 7.28 (t, 5H, J = 2.5 Hz), 7.18 (dd, 2H, J = 6.0, 4.3 Hz), 6.49 (d, 1H, J = 15.7 Hz), 6.29 (t, 1H, J = 5.9 Hz), 4.58 (s, 1H), 3.63−3.58 (m, 1H), 3.25 (q, 2H, J = 6.8 Hz), 2.85 (s, 1H), 2.64 (s, 1H), 1.77-0.86 (m, 10H). ^{13}CNMR (101 MHz, $CDCl_3$) δ_C 170.5, 165.0, 150.5, 142.5, 138.0, 136.5, 129.7, 128.6, 126.9, 125.7, 121.8, 48.2, 42.7, 39.9, 36.2, 36.2, 33.1, 32.1, 29.9, 24.1. MS *m/z* (ES$^+$) 392.4 [M+H]$^+$. HRMS $C_{24}H_{28}N_3O_2$ requires [M−H]$^-$ 390.2186, found [M−H]$^-$ 390.2187.

4-(1-(6-([1,1'-Biphenyl]-2-yloxy)hexyl)-1H-1,2,3-triazol-4-yl) pyridine (8).

12 (100 mg, 0.34 mmol) was dissolved in *tert*-butanol (2 mL), 4-ethynylpyridine (35 mg, 0.34 mmol), sodium ascorbate (27 mg, 0.14 mmol), $CuSO_4$ (2 mg, 1.36 × 10^{-2} mmol) and water (2 mL) were added under argon atmosphere. The mixture was stirred at 40 °C overnight under argon atmosphere. The reaction mixture was quenched with water (20 mL) and extracted with EtOAc (3 × 15 mL) and the organic phases were combined, dried over $MgSO_4$, filtered and concentrated under reduced pressure to provide a brown oil. The crude material was purified by CombiFlash® using acid method to afford the title compound (112 mg, 0.28 mmol, 82%) as a yellow oil. V_{max} (thin film, ATR)/ cm^{-1}: 3131, 3057, 3031, 2938, 2861, 1709, 1609, 1433, 1260, 1220, 1122, 1044, 991, 911, 753, 729, 698, 532. ^{1}HNMR (400 MHz, $CDCl_3$) δ_H 8.56 (s, 2H), 7.71 (s, 1H), 7.62 (d, 2H, J = 5.7 Hz), 7.48−7.40 (m, 2H), 7.33−7.15 (m, 5H), 6.98−6.83 (m, 2H), 4.21 (t, 2H, J = 7.2 Hz), 3.85 (t, 2H, J = 6.1 Hz), 1.78 (q, 2H, J = 7.3 Hz), 1.67−1.56 (m, 2H), 1.34 (dtd, 2H, J = 11.7, 9.0, 8.0, 6.1 Hz), 1.28-1.15 (m, 2H). ^{13}CNMR (101 MHz, $CDCl_3$) δ_C 155.9, 150.0, 145.0, 138.7, 138.6, 131.0, 131.0, 129.7, 128.8, 127.9, 126.9, 121.3, 121.1, 120.2, 112.7, 68.1, 50.4, 30.1, 28.9, 25.9, 25.4. MS *m/z* (ES$^+$) 399.4 [M+H]$^+$. HRMS $C_{25}H_{26}N_4ONa$ requires [M+Na]$^+$ 421.1983, found [M+Na]$^+$ 421.1999.

((2R,3S,4R,5S)-3,4-Dihydroxy-5-(4-((3-(4-(phenylsulfonyl) phenyl)ureido)methyl)phenyl)tetrahydrofuran-2-yl)methyldihydrogenphosphate (9a).

24a (56 mg, 0.08 mmol) was dissolved in anhydrous DCM (10 mL), TMSI (0.11 mL, 0.83 mmol) was added under argon atmosphere. The mixture was stirred at RT for 20 min under argon atmosphere and then MeOH (5 mL) was added. The mixture was stirred at RT for another 3 h and concentrated under reduced pressure to provide an orange oil. The crude material was purified by CombiFlash® using base method to afford the title compound (24 mg, 0.04 mmol, 50%) as a colourless oil. V_{max} (thin film, ATR)/cm^{-1}: 3325, 2953, 2173, 2155, 1698, 1683, 1590, 1542, 1337, 1227, 1159, 1107, 946, 733, 598, 583. ^{1}HNMR (400 MHz, CD$_3$OD) δ_H 7.94−7.87 (m, 2H), 7.82−7.74 (m, 2H), 7.65−7.49 (m, 5H), 7.40 (d, 2H, J = 8.1 Hz), 7.28 (d, 2H, J = 8.0 Hz), 4.68 (d, 1H, J = 6.9 Hz), 4.35 (s, 2H), 4.16 (dd, 1H, J = 5.4, 3.6 Hz), 4.09 (d, 1H, J = 4.2 Hz), 4.10-3.97 (m, 2H), 3.91 (dd, 1H, J = 6.9, 5.4 Hz). ^{13}CNMR (101 MHz, CD$_3$OD) δ_C 157.3, 146.6, 143.7, 140.8, 140.1, 134.5, 134.2, 130.5, 129.9, 128.3, 128.3, 127.8, 119.2, 85.2, 85.0 (d, J_{CP} = 8.8 Hz), 79.0, 73.2, 66.4 (d, J_{CP} = 5.2 Hz), 44.3. ^{31}PNMR (162 MHz, CD$_3$OD) δ_P 1.4 (s). MS m/z (ES$^+$) 579.2 [M+H]$^+$. HRMS C$_{25}$H$_{26}$N$_2$O$_{10}$PS requires [M−H]$^-$ 577.1048, found [M−H]$^-$ 577.1051.

((2R,3S,4R,5S)-5-(4-(3-(4-((8-Oxa-3-azabicyclo[3.2.1]octan-3-yl)sulfonyl)phenyl)ureido)methyl)phenyl)-3,4-dihydroxytetrahydrofuran-2-yl)methyldihydrogen phosphate (9b).

24b (109 mg, 0.15 mmol) was dissolved in anhydrous DCM (10 mL), TMSI (0.21 mL, 1.54 mmol) was added under argon atmosphere. The mixture was stirred at RT for 90 min under argon atmosphere and then MeOH (5 mL) was added. The mixture was stirred at RT for another 3 h and concentrated under reduced pressure to provide an orange oil. The crude material was purified by CombiFlash® using base method to afford the title compound (49 mg, 0.08 mmol, 53%) as a colourless oil. V_{max} (thin film, ATR)/cm^{-1}: 3336, 2921, 2155, 1698, 1589, 1541, 1446, 1319, 1229, 1152, 1107, 1018, 733, 593, 567. ^{1}HNMR (400 MHz, CD$_3$OD) δ_H 7.67−7.57 (m, 4H), 7.42 (d, 2H, J = 8.0 Hz), 7.33 (d, 2H, J = 7.9 Hz), 4.74 (d, 1H, J = 6.8 Hz), 4.38 (d, 4H, J = 4.3 Hz), 4.20 (t, 1H, J = 4.6 Hz), 4.14 (q, 1H, J = 4.3 Hz), 4.01 (dt, 3H, J = 12.5, 5.5 Hz), 3.34−3.26 (m, 2H), 2.54 (d, 2H, J = 11.2 Hz), 1.91 (d, 4H, J = 2.7 Hz). ^{13}CNMR (101 MHz, CD$_3$OD) δ_C 157.5, 145.9, 140.2, 139.7, 129.8, 128.4, 128.0, 127.9, 119.2, 85.0, 84.7 (d, J_{CP} = 8.8 Hz), 78.5, 75.0, 72.9, 65.9 (d, J_{CP} = 4.9 Hz), 52.1, 44.1, 28.4. ^{31}PNMR (162 MHz, CD$_3$OD) δ_P 2.1 (s). MS m/z (ES$^+$) 614.3 [M+H]$^+$. HRMS C$_{25}$H$_{31}$N$_3$O$_{11}$PS requires [M−H]$^-$ 612.1417, found [M−H]$^-$ 612.1422.

1-(4-((8-Oxa-3-azabicyclo[3.2.1]octan-3-yl)sulfonyl)phenyl)-3-(4(hydroxymethyl)benzyl)urea (10).

11 (100 mg, 0.26 mmol) was dissolved in THF (10 mL), (4-(aminomethyl)phenyl)methanol (35 mg, 0.26 mmol), imidazole (35 mg, 0.52 mmol) were added under argon atmosphere. The mixture was heated up to 50 °C and stirred overnight under argon atmosphere. The reaction mixture was extracted with EtOAc (3 × 30 mL) and the organic phases were combined, dried over MgSO$_4$, filtered and concentrated under reduced pressure to provide a yellow oil. The crude material was purified by CombiFlash® using acid method to afford the title compound (95 mg, 0.22 mmol, 85%) as a white solid. V_{max} (thin film, ATR)/cm^{-1}: 3410, 3322, 2976, 2867, 2359, 1672, 1542, 1509, 1205, 917, 733. 591, 577, 528. ^{1}HNMR (400 MHz, CDCl$_3$) δ_H 9.12 (s, 1H), 7.68−7.61 (m, 2H), 7.60−7.52 (m, 2H), 7.31−7.22 (m, 4H), 6.80 (t, 1H, J = 5.9 Hz), 5.13 (t, 1H, J = 5.7 Hz), 4.47 (d, 2H, J = 5.7 Hz), 4.31 (t, 4H, J = 4.6 Hz), 3.25-3.14 (m, 2H), 2.41 (dd, 2H, J = 11.4, 2.3 Hz), 1.86−1.74 (m, 4H). ^{13}CNMR (101 MHz, CDCl$_3$) δ_C 154.7, 145.0, 141.1, 138.3, 128.7, 126.9,

126.5, 126.2, 117.1, 72.7, 62.7, 50.9, 42.6, 27.4. MS m/z (ES$^+$) 432.4 [M+H]$^+$. HRMS C$_{21}$H$_{25}$N$_3$O$_5$SNa requires [M+Na]$^+$ 454.1390, found [M+Na]$^+$ 454.1407.

Phenyl (4-((8-oxa-3-azabicyclo[3.2.1]octan-3-yl)sulfonyl) phenyl)carbamate (11).

4-((8-Oxa-3-azabicyclo[3.2.1]octan-3-yl)sulfonyl)aniline (970 mg, 3.62 mmol) was dissolved in anhydrous THF (50 mL), phenyl chloroformate (1.36 mL, 10.86 mmol) and K$_2$CO$_3$ (2497 mg, 18.09 mmol) were add under argon atmosphere. The mixture was stirred for 3 h under argon atmosphere at RT. The reaction mixture was quenched with water (100 mL) and extracted with EtOAc (3 × 100 mL). The organic phases were combined, dried over MgSO$_4$, filtered and concentrated under reduced pressure to provide a yellow solid. The crude material was washed with cold Et$_2$O to afford the title compound (950 mg, 2.45 mmol, 68%) as a white solid. ^{1}HNMR (400 MHz, CDCl$_3$) δ_H 7.73−7.66 (m, 2H), 7.61 (d, 2H, J = 8.8 Hz), 7.46−7.37 (m, 2H), 7.34−7.23 (m, 2H), 7.23−7.16 (m, 2H), 4.36 (dd, 2H, J = 4.5, 2.3 Hz), 3.41−3.33 (m, 2H), 2.62 (dd, 2H, J = 11.2, 2.2 Hz), 2.06−1.88 (m, 4H). ^{13}CNMR (101 MHz, CDCl$_3$) δ_C 151.4, 150.3, 141.9, 130.3, 129.7, 129.2, 126.3, 121.7, 118.4, 73.8, 51.2, 27.9. MS m/z (ES$^+$) 389.4 [M+H]$^+$.

2-((6-Azidohexyl)oxy)-1,1'-biphenyl (12).

A solution of 6-([1,1'-biphenyl]-2-yloxy)hexan-1-ol (200 mg, 0.74 mmol) in anhydrous DMF (15 mL) was cooled down to 0 °C, DBU (0.33 mL, 2.22 mmol) and DPPA (0.48 mL, 2.22 mmol) were added under argon atmosphere. The mixture was stirred at 0 °C for 30 min under argon atmosphere and NaN$_3$ (144 mg, 2.22 mmol) was added. The mixture was heated up to 100 °C and stirred for 2 h under argon atmosphere. The reaction mixture was quenched with water (30 mL) and extracted with EtOAc (3 × 30 mL) and the organic phases were combined, dried over MgSO$_4$, filtered and concentrated under reduced pressure to provide a dark-brown oil. The crude material was purified by CombiFlash® using base method to afford the title compound (150 mg, 0.51 mmol, 69%) as a colourless oil. ^{1}HNMR (400 MHz, CDCl$_3$) δ_H 7.52−7.45 (m, 2H), 7.39−7.17 (m, 5H), 6.97 (td, 1H, J = 7.5, 1.2 Hz), 6.92 (dd, 1H, J = 8.2, 1.1 Hz), 3.91 (t, 2H, J = 6.3 Hz), 3.15 (t, 2H, J = 6.9 Hz), 1.66 (dt, 2H, J = 7.9, 6.2 Hz), 1.50 (q, 2H, J = 7.0 Hz), 1.32 (ttd, 4H, J = 15.2, 6.2, 4.6, 2.5 Hz). ^{13}CNMR (101 MHz, CDCl$_3$) δ_C 156.1, 138.8, 131.2, 131.0, 129.8, 128.7, 128.0, 127.0, 121.0, 112.7, 68.4, 51.5, 29.1, 28.9, 26.5, 25.9. MS characterization was not possible due to the poor ionisation.

(4-(4-Aminobutyl)piperidin-1-yl) (phenyl)methanone (13).

(4-(4-Azidobutyl)piperidin-1-yl) (phenyl)methanone (100 mg, 0.35 mmol) was dissolved in THF (10 mL), PPh$_3$ (139 mg, 0.53 mmol) and water (0.04 mL, 2.10 mmol) were added under argon atmosphere. The mixture was heated up to 75 °C and stirred for 3 h under argon atmosphere. The reaction mixture was quenched with water (30 mL) and extracted with EtOAc (3 × 20 mL) and the organic phases were combined, dried over MgSO$_4$, filtered and concentrated under reduced pressure to provide a colourless oil. The crude material was purified by CombiFlash® using acid method to afford the title compound (70 mg, 0.27 mmol, 77%) as a colourless oil. ^{1}HNMR (400 MHz, MeOD) δ_H 7.51−7.41 (m, 3H), 7.44−7.35 (m, 2H), 4.62 (d, 1H, J = 12.9 Hz), 3.71 (d, 1H, J = 13.3 Hz), 3.16−3.03 (m, 1H), 2.96−2.89 (m, 2H), 2.84 (t, 1H, J = 12.7 Hz), 1.86 (d, 1H, J = 13.2 Hz), 1.73−1.54 (m, 3H), 1.44 (dtd, 2H, J = 15.2, 7.1, 2.9 Hz), 1.38−1.27 (m, 2H), 1.16 (dd, 2H, J = 38.6, 19.2, 11.5 Hz). ^{13}CNMR (101 MHz, MeOD) δ_C 172.3, 137.3, 130.9,

129.7, 127.7, 49.3, 43.7, 40.7, 37.0, 36.8, 33.8, 33.0, 28.7, 24.5. MS *m/z* (ES$^+$) 261.4 [M+H]$^+$.

N-(4-(1-Benzoylpiperidin-4-yl)butyl)acrylamide (14).

13 (148 mg, 0.57 mmol) was dissolved in anhydrous DCM (20 mL), TEA (0.16 mL, 1.14 mmol) and acryloyl chloride (0.06 mL, 0.68 mmol) were added under argon atmosphere. The mixture was stirred for 30 min at RT under argon atmosphere. The reaction mixture was quenched with water (20 mL) and extracted with EtOAc (3 × 20 mL) and the organic phases were combined, dried over MgSO$_4$, filtered and concentrated under reduced pressure to provide a colourless oil. The crude material was purified by CombiFlash® using acid method to afford the title compound (107 mg, 0.34 mmol, 60%) as a colourless oil. ν_{max} (thin film, ATR)/cm^{-1}: 3289, 2929, 2856, 1610, 1545, 1438, 1280, 1485, 985, 708. ^{1}HNMR (400 MHz, CDCl$_3$) δ_H 7.41−7.31 (m, 5H), 6.24 (dd, 1H, *J* = 17.0, 1.6 Hz), 6.07 (dd, 1H, *J* = 17.0, 10.2 Hz), 5.99 (d, 1H, *J* = 6.3 Hz), 5.58 (dd, 1H, *J* = 10.2, 1.6 Hz), 4.65 (s, 1H), 3.70 (s, 1H), 3.28 (td, 2H, *J* = 7.3, 5.9 Hz), 2.93 (s, 1H), 2.72 (s, 1H), 1.84−1.72 (m, 1H), 1.66−1.55 (m, 1H), 1.55−0.91 (m, 8H). ^{13}CNMR (101 MHz, CDCl$_3$) δ_C 170.4, 165.7, 136.5, 131.1, 129.6, 128.5, 126.9, 126.2, 48.2, 42.6, 39.6, 36.2, 36.1, 33.0, 32.1, 29.9, 24.1. MS *m/z* (ES$^+$) 315.3 [M+H]$^+$. HRMS C$_{19}$H$_{26}$N$_2$O$_2$Na requires [M+Na]$^+$ 337.1868, found [M+Na]$^+$ 337.1886.

Phenyl (4-(phenylsulfonyl)phenyl)carbamate (16).

15 (4.92 g, 21.09 mmol) was dissolved in anhydrous THF (200 mL), phenyl chloroformate (13.23 mL, 105.43 mmol) and K$_2$CO$_3$ (0.87 g, 63.27 mmol) were add under argon atmosphere. The mixture was stirred for 20 min at RT under argon atmosphere. The reaction mixture was quenched with water (50 mL) and extracted with EtOAc (3 × 150 mL). The organic phases were combined, dried over MgSO$_4$, filtered and concentrated under reduced pressure to provide a brown solid. The crude material was purified by flash chromatography (silica gel), eluting with 1% MeOH in DCM to afford the title compound (6.40 g, 18.14 mmol, 86%) as a white solid. ^{1}HNMR (400 MHz, (CD$_3$)$_2$SO) δ_H 10.76 (s, 1H), 7.97−7.90 (m, 4H), 7.77−7.70 (m, 2H), 7.69−7.57 (m, 3H), 7.43 (t, 2H, *J* = 7.8 Hz), 7.31−7.20 (m, 3H). ^{13}CNMR (101 MHz, (CD$_3$)$_2$SO) δ_C 151.6, 150.2, 143.6, 141.7, 134.5, 133.4, 129.7, 129.5, 128.9, 127.0, 125.7, 121.9, 118.5. MS *m/z* (ES$^+$) 354.1 [M+H]$^+$.

4-((3R,4R,5R)-3,4-Bis(benzyloxy)-5-((benzyloxy)methyl)-2-hydroxytetrahydrofuran-2-yl)benzonitrile (18).

A solution of 4-iodobenzonitrile (109 mg, 0.48 mmol) in anhydrous THF (8 mL) was cooled down to −78 °C and *i*-PrMgCl·LiCl (0.37 mL from a 1.3 mol/L solution in THF, 0.48 mmol) was added dropwise under argon atmosphere. The reaction mixture was stirred for 1 h under −78 °C to form the yellow turbo Grignard solution. The ribonolactone **17** (100 mg, 0.24 mmol) anhydrous THF solution (2 mL) was added to the Grignard solution dropwise and stirred overnight under argon atmosphere at RT. The reaction mixture was quenched with water (80 mL) and extracted with EtOAc (3 × 100 mL). The organic phases were combined, dried over MgSO$_4$, filtered and concentrated under reduced pressure to provide a yellow oil. The crude material was taken forward without further purification. MS *m/z* (ES$^+$) 544.3 [M+Na]$^+$.

4-((2S,3S,4R,5R)-3,4-Bis(benzyloxy)-5-((benzyloxy)methyl)tetrahydrofuran-2-yl)benzonitrile (19).

A solution of crude **18** (0.24 mmol as hypothetic quantitative yield from last step) in anhydrous DCM (15 mL) was cooled down to −78 °C, BF$_3$·Et$_2$O (0.19 mL, 0.72 mmol) and TES (0.12 mL, 0.72 mmol) were added dropwise under argon atmosphere. The

mixture was stirred for 1 h at −78 °C and then allowed to reach RT and stirred overnight under argon atmosphere. The reaction mixture was quenched with a saturated NaHCO$_3$ aqueous solution (50 mL) and extracted with EtOAc (3 × 30 mL). The organic phases were combined, dried over MgSO$_4$, filtered and concentrated under reduced pressure to provide a pink oil. The crude material was purified by CombiFlash® using acid method to afford the title compound (60 mg, 0.12 mmol, 50% over two steps) as a colourless oil. ^{1}HNMR (400 MHz, CDCl$_3$) δ_H 7.49 (d, 2H, *J* = 8.4 Hz), 7.44 (d, 2H, *J* = 8.2 Hz), 7.35−7.06 (m, 15H), 4.98 (d, 1H, *J* = 7.2 Hz), 4.59−4.24 (m, 7H), 3.98 (dd, 1H, *J* = 5.1, 3.3 Hz), 3.71 (dd, 1H, *J* = 7.3, 5.0 Hz), 3.63 (dd, 1H, *J* = 10.4, 3.9 Hz), 3.56 (dd, 1H, *J* = 10.4, 3.5 Hz). ^{13}CNMR (101 MHz, CDCl$_3$) δ_C 146.2, 138.0, 137.8, 137.5, 132.2, 128.6, 128.5, 128.3, 128.1, 128.0, 128.0, 127.9, 127.8, 127.0, 119.1, 111.4, 84.0, 82.4, 81.6, 77.4, 73.7, 72.6, 72.1, 70.5. MS *m/z* (ES$^+$) 506.4 [M+H]$^+$.

4-((2S,3R,4S,5R)-3,4-Dihydroxy-5-(hydroxymethyl)tetrahydrofuran-2-yl)benzonitrile (20).

19 (790 mg, 1.56 mmol) was dissolved in anhydrous DCM (30 mL) and BBr$_3$ (6.26 mL from a 1 mol/L solution in DCM, 6.26 mmol) was added under argon atmosphere. The mixture was stirred for 1 h under argon atmosphere at 0 °C. The reaction mixture was quenched with MeOH (10 mL) and concentrated under reduced pressure to provide a dark-yellow oil. The crude material was purified by CombiFlash® using acid method to afford the title compound (261 mg, 1.11 mmol, 71%) as a colourless oil. ν_{max} (thin film, ATR)/cm^{-1}: 3449, 2932, 2883, 2232, 1610, 1411, 1332, 1114, 1055, 827, 561. ^{1}HNMR (400 MHz, CDCl$_3$) δ_H 7.70 (d, 2H, *J* = 8.4 Hz), 7.65 (d, 2H, *J* = 8.4 Hz), 4.76 (d, 1H, *J* = 7.1 Hz), 4.08−3.97 (m, 2H), 3.85−3.76 (m, 2H), 3.72 (dd, 1H, *J* = 12.0, 4.6 Hz). ^{13}CNMR (101 MHz, CDCl$_3$) δ_C 148.1, 133.1, 128.0, 119.8, 112.2, 86.9, 84.3, 79.3, 73.0, 63.5. MS *m/z* (ES$^+$) 234.2 [M−H]$^-$. HRMS C$_{12}$H$_{12}$NO$_4$ requires [M−H]$^-$ 234.0769, found [M−H]$^-$ 234.0772.

4-((3aS,4S,6R,6aR)-6-(Hydroxymethyl)-2,2-dimethyltetrahydrofuro[3,4-d][1,3]dioxol-4-yl)benzonitrile (21).

20 (89 mg, 0.38 mmol) was dissolved in anhydrous MeCN (15 mL), ZrCl$_4$·THF$_2$ (29 mg, 0.08 mmol) and DMP (0.14 mL, 1.14 mmol) were added under argon atmosphere. The mixture was stirred for 1 h under argon atmosphere at RT. The reaction mixture was quenched with a saturated NaHCO$_3$ aqueous solution (30 mL) and extracted with EtOAc (3 × 20 mL). The organic phases were combined, dried over MgSO$_4$, filtered and concentrated under reduced pressure to provide a yellow oil. The crude material was purified by CombiFlash® using base method to afford the title compound (77 mg, 0.28 mmol, 74%) as a colourless oil. ν_{max} (thin film, ATR)/cm^{-1}: 3483, 2936, 2881, 2342, 2229, 1611, 1382, 1212, 1156, 1077, 857, 829, 558. ^{1}HNMR (400 MHz, CDCl$_3$) δ_H 7.68−7.62 (m, 2H), 7.51 (d, 2H, *J* = 8.2 Hz), 4.90 (d, 1H, *J* = 5.7 Hz), 4.74 (dd, 1H, *J* = 6.9, 4.1 Hz), 4.46 (dd, 1H, *J* = 6.9, 5.7 Hz), 4.21 (q, 1H, *J* = 3.9 Hz), 3.95 (dd, 1H, *J* = 12.2, 3.2 Hz), 3.82 (d, 1H, *J* = 12.1 Hz), 1.85 (s, 1H), 1.62 (s, 3H), 1.36 (s, 3H). ^{13}CNMR (101 MHz, CDCl$_3$) δ_C 145.0, 132.5, 126.4, 118.9, 115.6, 111.9, 86.7, 85.1, 84.7, 81.6, 62.9, 27.7, 25.6. MS *m/z* (ES$^+$) 274.3 [M−H]$^-$. HRMS C$_{15}$H$_{17}$NO$_4$Na requires [M+Na]$^+$ 298.1037, found [M+Na]$^+$ 298.1050.

((3aR,4R,6S,6aS)-6-(4-Cyanophenyl)-2,2-dimethyltetrahydrofuro[3,4-d][1,3]dioxol-4-yl)methyl diethyl phosphate (22).

21 (68 mg, 0.25 mmol) was dissolved in anhydrous THF (15 mL), NMI (0.12 mL, 1.48 mmol) and diethyl phosphorochloridate (0.11 mL, 0.74 mmol) were added under argon

atmosphere. The mixture was stirred overnight under argon atmosphere at RT. The reaction mixture was quenched with water (20 mL) and extracted with EtOAc (3 × 20 mL) and the organic phases were combined, dried over MgSO$_4$, filtered and concentrated under reduced pressure to provide a yellow oil. The crude material was purified by CombiFlash® using base method to afford the title compound (98 mg, 0.24 mmol, 96%) as a colourless oil. ν_{max} (thin film, ATR)/cm^{-1}: 2985, 2937, 2908, 2228, 1611, 1373, 1264, 1213, 1078, 1023, 979, 813, 557, 511. ^{1}HNMR (400 MHz, CDCl$_3$) δ_H 7.67−7.60 (m, 2H), 7.52 (d, 2H, J = 8.1 Hz), 4.91 (d, 1H, J = 5.5 Hz), 4.74 (dd, 1H, J = 6.7, 3.5 Hz), 4.45 (dd, 1H, J = 6.7, 5.5 Hz), 4.36−4.18 (m, 3H), 4.11 (p, 4H, J = 7.3 Hz), 1.62 (s, 3H), 1.37−1.28 (m, 9H). ^{13}CNMR (101 MHz, CDCl$_3$) δ_C 145.1, 132.4, 126.4, 118.9, 115.5, 111.8, 86.7, 85.3, 82.7 (d, J_{CP} = 7.7 Hz), 81.6, 66.8 (d, J_{CP} = 5.7 Hz), 64.2, 64.2, 27.7, 25.7, 16.3, 16.2. ^{31}PNMR (162 MHz, CDCl$_3$) δ_P −0.9 (s). MS m/z (ES$^+$) 412.4 [M+H]$^+$. HRMS C$_{19}$H$_{26}$NO$_7$PNa requires [M+Na] 434.1322, found [M+Na] 434.1339.

((3aR,4R,6S,6aS)-6-(4-(Aminomethyl)phenyl)-2,2-dimethyltetrahydrofuro[3,4-d][1,3]dioxol-4-yl)methyl diethyl phosphate (23).

22 (88 mg, 0.21 mmol) was dissolved in THF (13 mL) and BH$_3$·THF (2.14 mL from a 1 mol/L solution in THF, 2.14 mmol) was added under argon atmosphere. The mixture was heated up to 60 °C and stirred overnight under argon atmosphere. The reaction mixture was quenched with MeOH (8 mL) and concentrated under reduced pressure to provide a colourless oil. The crude material was taken forward without further purification. MS m/z (ES$^+$) 416.4 [M+H]$^+$.

((3aR,4R,6S,6aS)-2,2-Dimethyl-6-(4-((3-(4-(phenylsulfonyl) phenyl)ureido)methyl)phenyl)tetrahydrofuro[3,4-d][1,3]dioxol-4-yl)methyldiethyl phosphate (24a).

The crude **23** (0.21 mmol as hypothetic quantitative yield from last step) was dissolved in EtOAc (15 mL), K$_2$CO$_3$ (89 mg, 0.64 mmol), **16** (151 mg, 0.43 mmol) and water (5 mL) were added under argon atmosphere. The mixture was heated up to 70 °C and stirred for 1 h under argon atmosphere. The reaction mixture was extracted with EtOAc (3 × 30 mL) and the organic phases were combined, dried over MgSO$_4$, filtered and concentrated under reduced pressure to provide a yellow oil. The crude material was purified by CombiFlash® using base method to afford the title compound (75 mg, 0.11 mmol, 52% over two steps) as a colourless oil. ν_{max} (thin film, ATR)/cm^{-1}: 3356, 2986, 2935, 1703, 1590, 1539, 1305, 1244, 1153, 1106, 1027, 839, 732, 689, 592, 566. ^{1}HNMR (400 MHz, CDCl$_3$) δ_H 8.25 (s, 1H), 7.85 (dd, 2H, J = 7.3, 1.8 Hz), 7.71−7.63 (m, 2H), 7.56−7.41 (m, 5H), 7.24 (s, 1H), 7.17 (d, 2H, J = 8.0 Hz), 6.12 (t, 1H, J = 5.6 Hz), 4.84 (d, 1H, J = 4.9 Hz), 4.64 (dd, 1H, J = 6.9, 3.8 Hz), 4.44 (dd, 1H, J = 6.8, 4.9 Hz), 4.39−4.12 (m, 5H), 4.05 (p, 4H, J = 7.2 Hz), 1.59 (s, 3H), 1.34−1.19 (m, 9H). ^{13}CNMR (101 MHz, CDCl$_3$) δ_C 155.3, 145.0, 142.3, 138.9, 138.5, 133.1, 133.0, 129.4, 129.1, 127.8, 127.4, 126.1, 118.1, 115.4, 87.0, 85.8, 82.5 (d, J_{CP} = 7.3 Hz), 81.2, 67.2 (d, J_{CP} = 5.9 Hz), 64.5, 64.5, 43.8, 27.6, 25.6, 16.2, 16.2. ^{31}PNMR (162 MHz, CDCl$_3$) δ_P −1.6 (s). MS m/z (ES$^+$) 675.3 [M+H]$^+$. HRMS C$_{32}$H$_{39}$N$_2$O$_{10}$PSNa requires [M+Na] 697.1931, found [M+Na] 697.1955.

((3aR,4R,6S,6aS)-6-(4-((3-(4-((8-Oxa-3-azabicyclo[3.2.1] octan-3-yl)sulfonyl)phenyl)ureido)methyl)phenyl)-2,2-dimethyltetrahydrofuro[3,4-d][1,3]dioxol-4-yl)methyl-diethylphosphate (24b).

The crude **23** (0.14 mmol as hypothetic quantitative yield from last step) was dissolved in THF (10 mL), **11** (62 mg, 0.16 mmol)

and imidazole (18 mg, 0.26 mmol) were added under argon atmosphere. The mixture was heated up to 60 °C and stirred for 3 h under argon atmosphere. The reaction mixture was extracted with EtOAc (3 × 30 mL) and the organic phases were combined, dried over MgSO$_4$, filtered and concentrated under reduced pressure to provide a yellow oil. The crude material was purified by CombiFlash® using acid method to afford the title compound (62 mg, 0.09 mmol, 56% over two steps) as a colorless oil. ν_{max} (thin film, ATR)/cm^{-1}: 3359, 2983, 2957, 2909, 2247, 1702, 1591, 1538, 1349, 1216, 1159, 1105, 1023, 946, 729, 582, 493. ^{1}HNMR (400 MHz, CDCl$_3$) δ_H 8.28 (s, 1H), 7.55 (d, 2H, J = 9.0 Hz), 7.49 (d, 2H, J = 9.0 Hz), 7.28 (d, 2H, J = 8.2 Hz), 7.21 (d, 2H, J = 8.0 Hz), 6.12 (t, 1H, J = 5.4 Hz), 4.85 (d, 1H, J = 4.9 Hz), 4.65 (dd, 1H, J = 6.8, 3.7 Hz), 4.45 (dd, 1H, J = 6.8, 4.9 Hz), 4.40−4.13 (m, 7H), 4.07 (p, 4H, J = 7.2 Hz), 3.29 (dd, 2H, J = 11.0, 4.4 Hz), 2.55 (dt, 2H, J = 11.1, 2.2 Hz), 1.94 (ddd, 4H, J = 17.5, 12.5, 8.0, 3.9 Hz), 1.59 (s, 3H), 1.34−1.27 (m, 9H). ^{13}CNMR (101 MHz, CDCl$_3$) δ_C 155.4, 144.7, 138.8, 138.5, 129.0, 127.8, 127.1, 126.1, 117.7, 115.4, 86.9, 85.8, 82.4 (d, J_{CP} = 7.3 Hz), 81.1, 73.8, 67.2 (d, J_{CP} = 5.8 Hz), 64.6, 64.5, 51.2, 27.9, 27.6, 25.6, 16.3, 16.2. ^{31}PNMR (162 MHz, CDCl$_3$) δ_P −1.6 (s). MS m/z (ES$^+$) 710.3 [M+H]$^+$. HRMS C$_{32}$H$_{22}$N$_3$O$_{11}$PSNa requires [M+Na]$^+$ 732.2301, found [M+Na]$^+$ 732.2326.

Author contributions

Siyuan Tang and Sam Butterworth conceptualised the research. Siyuan Tang conducted chemical synthesis and structural characterisation under the supervision of Sam Butterworth. *In vitro* assays were performed by Siyuan Tang, Oliver Smith, Miguel Garzon Sanz and Daniel Egbase under the supervision of Sam Butterworth and Paul Caton. Molecular modelling studies were conducted by Siyuan Tang. Crystallography was conducted and analysed by Andreas Krämer under the supervision of Stefan Knapp. Siyuan Tang, Miguel Garzon Sanz, Oliver Smith and Sam Butterworth were involved in data interpretation and discussion. Sam Butterworth and Siyuan Tang co-wrote the manuscript with input from Andreas Krämer and Stefan Knapp. All authors approved the final version of the manuscript.

Conflicts of interest

The authors declare no conflicts of interest.

Appendix A.   Supporting information

Supporting data to this article can be found online at https://doi.org/10.1016/j.apsb.2022.07.016.

References

1. Cantó C, Menzies K, Auwerx J. NAD+ metabolism and the control of energy homeostasis—a balancing act between mitochondria and the nucleus. *Cell Metab* 2015;**22**:31−53.
2. Covarrubias AJ, Perrone R, Grozio A, Verdin E. NAD+ metabolism and its roles in cellular processes during ageing. *Nat Rev Mol Cell Biol* 2021;**22**:119−41.
3. Mouchiroud L, Houtkooper RH, Moullan N, Katsyuba E, Ryu D, Cantó C, et al. The NAD+/Sirtuin pathway modulates longevity through activation of mitochondrial UPR and FOXO signaling. *Cell* 2013;**154**:430.
4. Burgos ES, Ho MC, Almo SC, Schramm VL. A phosphoenzyme mimic, overlapping catalytic sites and reaction coordinate motion for human NAMPT. *Proc Natl Acad Sci U S A* 2009;**106**:1−6.
5. Kennedy BE, Sharif T, Martell E, Dai C, Kim Y, Lee PWK, et al. NAD+ salvage pathway in cancer metabolism and therapy. *Pharmacol Res* 2016;**114**:274−83.
6. Amici A, Grolla AA, Del Grosso E, Bellini R, Bianchi M, Travelli C, et al. Synthesis and degradation of adenosine 5′-tetraphosphate by nicotinamide and nicotinate phosphoribosyltransferases. *Cell Chem Biol* 2017;**24**:553−564.e4.
7. Wang B, Hasan MK, Alvarado E, Yuan H, Wu H, Chen WY. NAMPT overexpression in prostate cancer and its contribution to tumor cell survival and stress response. *Oncogene* 2011;**30**:907−21.
8. Gunzner-Toste J, Zhao G, Bauer P, Baumeister T, Buckmelter AJ, Caligiuri M, et al. Discovery of potent and efficacious urea-containing nicotinamide phosphoribosyltransferase (NAMPT) inhibitors with reduced CYP2C9 inhibition properties. *Bioorg Med Chem Lett* 2013;**23**:3531−8.
9. Hasmann M, Schemainda I. FK866, a highly specific noncompetitive inhibitor of nicotinamide phosphoribosyltransferase, represents a novel mechanism for induction of tumor cell apoptosis. *Cancer Res* 2003;**63**:7436−42.
10. Oh A, Ho YC, Zak M, Liu Y, Chen X, Yuen PW, et al. Structural and biochemical analyses of the catalysis and potency impact of inhibitor phosphoribosylation by human nicotinamide phosphoribosyltransferase. *Chembiochem* 2014;**15**:1121−30.
11. Zheng X, Bauer P, Baumeister T, Buckmelter AJ, Caligiuri M, Clodfelter KH, et al. Structure-based identification of ureas as novel nicotinamide phosphoribosyltransferase (Nampt) inhibitors. *J Med Chem* 2013;**56**:4921−37.
12. Wilsbacher JL, Cheng M, Cheng D, Trammell SAJ, Shi Y, Guo J, et al. Discovery and characterization of novel nonsubstrate and substrate NAMPT inhibitors. *Mol Cancer Ther* 2017;**16**:1236−45.
13. Goldinger SM, Bischof SG, Fink-Puches R, Klemke CD, Dréno B, Bagot M, et al. Efficacy and safety of Apo 866 in patients with refractory or relapsed cutaneous T-cell lymphoma: a phase 2 clinical trial. *JAMA Dermatology* 2016;**152**:837−9.
14. Wang G, Han T, Nijhawan D, Theodoropoulos P, Naidoo J, Yadavalli S, et al. P7C3 neuroprotective chemicals function by activating the rate-limiting enzyme in NAD salvage. *Cell* 2014;**158**:1324−34.
15. Gardell SJ, Hopf M, Khan A, Dispagna M, Sessions EH, Falter R, et al. Boosting NAD+ with a small molecule that activates NAMPT. *Nat Commun* 2019;**10**:3241.
16. Pieper AA, Xie S, Capota E, Estill SJ, Zhong J, Jeffrey M, et al. Discovery of a Pro-Neurogenic, neuroprotective chemical. *Cell* 2010;**142**:39−51.
17. Pinkerton AB, Sessions EH, Hershberger P, Maloney PR, Peddibhotla S, Hopf M, et al. Optimization of a urea-containing series of nicotinamide phosphoribosyltransferase (NAMPT) activators. *Bioorg Med Chem Lett* 2021;**41**:28007.
18. Akiu M, Tsuji T, Sogawa Y, Terayama K, Yokoyama M, Tanaka J, et al. Discovery of 1-[2-(1-methyl-1*H*-pyrazol-5-yl)-[1,2,4]triazolo[1,5-*a*]pyridin-6-yl]-3-(pyridin-4-ylmethyl)urea as a potent NAMPT (nicotinamide phosphoribosyltransferase) activator with attenuated CYP inhibition. *Bioorg Med Chem Lett* 2021;**43**:128048.
19. Akiu M, Tsuji T, Iida K, Sogawa Y, Terayama K, Yokoyama M, et al. Discovery of DS68702229 as a potent, orally available NAMPT (nicotinamide phosphoribosyltransferase) activator. *Chem Pharm Bull* 2021;**69**:1110−22.
20. Wang L, Liu M, Zu Y, Yao H, Wu C, Zhang R, et al. Optimization of NAMPT activators to achieve *in vivo* neuroprotective efficacy. *Eur J Med Chem* 2022;**236**:114260.
21. Zhang RY, Qin Y, Lv XQ, Wang P, Xu TY, Zhang L, et al. A fluorometric assay for high-throughput screening targeting nicotinamide phosphoribosyltransferase. *Anal Biochem* 2011;**412**:8−25.
22. Burgos ES, Ho MC, Almo SC, Schramm VL. A phosphoenzyme mimic, overlapping catalytic sites and reaction coordinate motion for human NAMPT. *Proc Natl Acad Sci U S A* 2009;**106**:13748−53.
23. Jerome A, Claude B, Monsif B, Romain C, Sandrine H, Samir J, inventors, Sanofi SA, assignee. *Nicotinamide derivatives, preparation thereof, and therapeutic use thereof as anticancer drugs*. PCT WO2010109122; 2010.
24. Cheng H, Bagrodia S, Bailey S, Edwards M, Hoffman J, Hu Q, et al. Discovery of the highly potent PI3K/MTOR dual inhibitor PF-04691502 through structure based drug design. *Medchemcomm* 2010;**1**:139−44.
25. Sayers SR, Beavil RL, Fine NHF, Huang GC, Choudhary P, Pacholarz KJ, et al. Structure-functional changes in ENAMPT at high concentrations mediate mouse and human beta cell dysfunction in type 2 diabetes. *Diabetologia* 2020;**63**:313−23.
26. Galli U, Ercolano E, Carraro L, Blasi Roman CR, Sorba G, Canonico PL, et al. Synthesis and biological evaluation of isosteric analogues of FK866, an inhibitor of NAD salvage. *ChemMedChem* 2008;**3**:771−9.
27. Travelli C, Aprile S, Rahimian R, Grolla AA, Rogati F, Bertolotti M, et al. Identification of novel triazole-based nicotinamide phosphoribosyltransferase (NAMPT) inhibitors endowed with antiproliferative and antiinflammatory activity. *J Med Chem* 2017;**60**:1768−92.
28. Bonnac LF, Gao GY, Chen L, Patterson SE, Jayaram HN, Pankiewicz KW. Efficient synthesis of benzamide riboside, a potential anticancer agent. *Nucleos Nucleot Nucleic Acids* 2007;**26**:1249−53.
29. Krohn K, Heins H, Wielckens K. Synthesis and cytotoxic activity of C-glycosidic nicotinamide riboside analogs. *J Med Chem* 1992;**35**:511−7.
30. Hernández AR, Kool ET. The components of XRNA: synthesis and fluorescence of a full genetic set of size-expanded ribonucleosides. *Org Lett* 2011;**13**:676−9.
31. Singh S, Duffy CD, Shah STA, Guiry PJ. ZrCl$_4$ as an efficient catalyst for a novel one-pot protection. *J Org Chem* 2008;**73**:6429−32.
32. Zhou L, Zhang H, Tao S, Ehteshami M, Cho JH, McBrayer TR, et al. Synthesis and evaluation of 2,6-modified purine 2′-C-methyl ribonucleosides as inhibitors of HCV replication. *ACS Med Chem Lett* 2016;**7**:17−22.
33. Burkhardt ER, Matos K. Boron reagents in process chemistry: excellent tools for selective reductions. *Chem Rev* 2006;**106**:2617−50.
34. Jung ME, Lyster MA. Quantitative dealkylation of alkyl ethers *via* treatment with trimethylsilyl iodide. A new method for ether hydrolysis. *J Org Chem* 1977;**42**:3761−4.
35. Jung ME, Lyster MA. Cleavage of methyl ethers with iodotrimethylsilane: cyclohexanol from cyclohexyl methyl ether. *Org Synth* 2003;**6**:35.